FOI-R--1047--SE
November 2003
ISSN 1650-1942
Scientific report

RAYLAB

- a ray tracing program in underwater acoustics

Leif Abrahamsson

Systems Technology
SE-172 90 Stockholm

SWEDISH DEFENCE RESEARCH AGENCY

Systems Technology
SE-172 90 Stockholm

FOI-R--1047--SE

November 2003

ISSN 1650-1942

Scientific report

RAYLAB

- a ray tracing program in underwater acoustics

Leif Abrahamsson

Issuing organization	Report number, ISRN	Report type
FOI – Swedish Defence Research Agency Systems Technology SE-172 90 Stockholm	FOI-R--1047--SE	Scientific report
	Research area code 4. C4ISR	
	Month year November 2003	**Project no.** E6051
	Customers code 5. Commissioned Research	
	Sub area code 43 Underwater Sensors	

Author/s (editor/s)	Project manager
Leif Abrahamsson	Peter Krylstedt
	Approved by Monica Dahlén
	Sponsoring agency Swedish Armed Forces
	Scientifically and technically responsible Leif Abrahamsson

Report title

RAYLAB - a ray tracing program in underwater acoustics

Abstract (not more than 200 words)

RAYLAB is a ray tracing program tailor-made for inversion analysis of experimental data to determine geoacoustic parameters of a multilayered seabottom. The most important features are the computation of sub-bottom eigenrays and the partition of transmission loss into factors due to geometrical spread, absorption and reflection losses at sediment interfaces. Fast computational speed has been an important aspect in the numerical treatment, since it is a critical factor of inversion schemes for sediment classification in real time.

The report is a documentation of the theoretical and numerical ray model in RAYLAB.

Keywords

underwater acoustics, ray theory, ray tracing program, Helmholtz equation, inversion analysis

Further bibliographic information	Language English
ISSN 1650-1942	**Pages** 35 p.
	Price acc. to pricelist

Utgivare	Rapportnummer, ISRN	Klassificering
Totalförsvarets Forskningsinstitut - FOI Systemteknik 172 90 Stockholm	FOI-R--1047--SE	Vetenskaplig rapport
	Forskningsområde 4. Spaning och ledning	
	Månad, år November 2003	**Projektnummer** E6051
	Verksamhetsgren 5. Uppdragsfinansierad verksamhet	
	Delområde 43 Undervattenssensorer	

Författare/redaktör	Projektledare
Leif Abrahamsson	Peter Krylstedt
	Godkänd av Monica Dahlén
	Uppdragsgivare/kundbeteckning Försvarsmakten
	Tekniskt och/eller vetenskapligt ansvarig Leif Abrahamsson

Rapportens titel (i översättning)

RAYLAB - ett strålgångsprogram i hydroakustik

Sammanfattning (högst 200 ord)

RAYLAB är ett strålgångsprogram skräddarsytt för inversionsanalys av data från vågutbredningsexperiment för att bestämma geoakustiska parametrar i en havsbotten bestående av flera sedimentskikt. De viktigaste egenskaperna hos RAYLAB är beräkningen av egenstrålar i sedimenten och uppdelningen av transmissionsförluster i faktorer som beror av geometrisk spridning, absorption och reflektionsförluster i gränsytor mellan sediment. Korta beräkningstider har varit en viktig aspekt in den numeriska behandlingen, eftersom detta är en kritisk faktor i inversionsscheman för sedimentklassificering i realtid.

Rapporten är en dokumentation av den teoretiska och numeriska strålgångsmodellen i RAYLAB.

Nyckelord

hydroakustik, strålgångsteori, strålgångsprogram, Helmholtz ekvation, inversionsanalys

Övriga bibliografiska uppgifter	Språk Engelska
ISSN 1650-1942	**Antal sidor:** 35 s.
Distribution enligt missiv	**Pris: Enligt prislista**

FOI1004 Utgåva 11 2002.02 www.signon.se Sign On AB

Contents

1 Introduction

The development of RAYLAB is motivated by the need to simulate the propagation of broadband acoustic signals in the seabed for sediment classification in real time. The probing sonar system would be mounted on a tow-fish operating quite close to the bottom. The transmitted pulses would be directed almost vertically and received by a towed array some $20 - 100m$ behind the tow-fish. Extraordinary computational speed is needed for inversion under transit. Forward modeling in a fraction of a second can only be achieved by a ray model. RAYLAB is an implementation of classical ray theory, in which computational speed has received a high priority. Features of importance for inversion are bottom penetrating eigenrays, and the separation of transmission loss into geometrical spread, absorption and reflection losses at sediment interfaces.

RAYLAB is limited to range-independent environments as opposed to many other ray tracing codes. The computational simplifications offered in the range-independent case are vast, as will be made evident in this work.

This report is a thorough account of the theoretical and numerical ray model in RAYLAB. Although most of the derivations can be found in the literature, it is convenient to have a compiled documentation. The numerical technique of finding the eigenrays is treated in more detail than is commonly done elsewhere. The topic is written in mathematical terms, and it is mainly of interest for those who intend to develope wave propagation models. Nevertheless it is also important to make a software tool like RAYLAB accessible to practitioners of wave propagation models in sonar applications. It should be recognized, that the design of the computational model, and how to use it in the applied fields, are two quite different disciplines. Therefore we found it worthwhile to make a user oriented presentation of ray theory and the scope of RAYLAB. Thus Sec. 2 is an outline of what a ray code can offer as a simulation tool in underwater acoustics. It is done by means of a number of pictorial illustrations. Information on the operational use of RAYLAB is given by the user's guide, which is prepared as a separate document.

2 Illustrative examples

2.1 An acoustic model for all ages

There is a variety of wave propagation models in acoustics. In practice the very simplest one, sound propagation along a straight line from the source to the receiver, may be better than anything else. To illustrate this point, I will tell a story from my childhood.

I grew up in a rural area which was plagued by thunderstorms in the summer. We were a group of neighbor boys with a playground of wide fields and deep forests. Trees, devastated by lightning, could be seen all around. Being far from home, we learned to cope with the danger by keeping track of the thunderfront using the speed of sound. At the view of a lightning all work stopped and turned into a unisonous count of the seconds to the arrival of the boom. A boom within three counts was an emergency, and we would run for life to the nearest barn. Standing in the middle of the barn, we waited for the inferno to pass. Once one of the walls cracked by a strike of lightning.

The counting continued, but now for a reversed and equally important purpose. A boom on three or more was a signal to return to the field activities. We had already been halted too long.

The simple model of relating speed, time and distance along a straight line has also been put to good use in professional applications like echo sounders and ultrasonic imaging. However, there are many cases of practical interest in which the straight line model is insufficient, because wave phenomena like refraction and diffraction are neglected. A natural extension is ray theory, a classical discipline of both acoustics and optics.

2.2 Fermat's principle and Snell's law

According to Fermat's principle of least time, sound will take the fastest way between a source and a receiver, which is not necessarily the same as the shortest one, that is, the straight line. This distinction may be important when the speed of sound varies. The sound waves will make a detour (refract) in a region of higher velocity before turning towards the receiver. The straight line connection would be too slow. Whether curved paths are important or not depends on how much the speed of sound varies transversely to the direction of propagation.

When a sound wave encounters an interface between two different media, the wave is partially reflected as well as transmitted. The angles of the incident, reflected and transmitted waves θ_i, θ_r and θ_t with respect to the normal of the interface obey Snell's law

$$\theta_i = \theta_r \quad \text{and} \quad \frac{\sin\theta_i}{c_i} = \frac{\sin\theta_t}{c_t},$$

where c_i and c_t denote the speed of sound on either side of the boundary. Actually, Snell's law is a simplified model of a complicated wave interaction around the media discontinuity. From a practical point of view though, Snell's law is accurate enough for a wide range of applications.

The wave phenomena as expressed by Fermat's principle and Snell's law are closely related. Both are well reproduced in ray acoustics, as demonstrated in Sec. 2.4-6.

2.3 An example of a geoacoustic profile

In underwater acoustics the sea and bottom sediments often exhibit considerable variations of the speed of sound by depth. Figure 2.1 shows a sound speed profile from a field trial in August 2002 in the Baltic Sea.

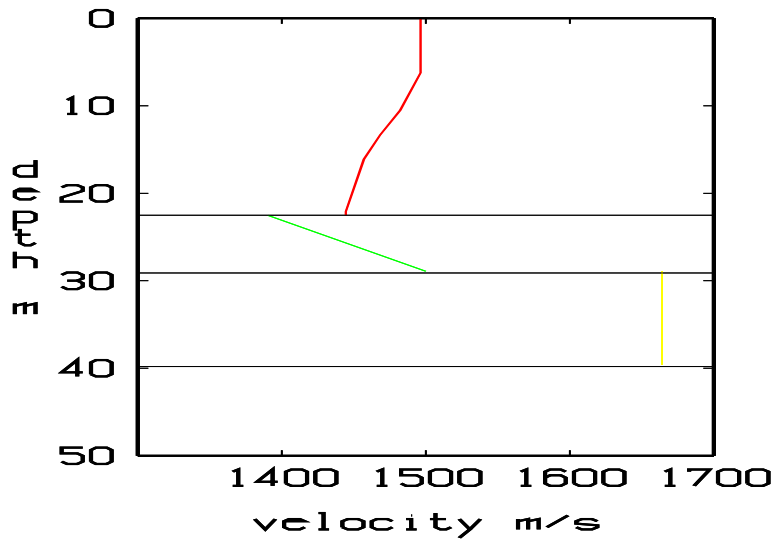

Figure 2.1: *The sound speed profile of the water (red), the top sediment (green) and the bottom sediment (yellow). The velocity of the bedrock below a depth of around* 40m *was set to* 5200m/s.

The water depth (22.5 m) as well as the sound velocity of the water were measured. The speed and thicknesses of the two bottom sediments were determined by an inversion analysis [1] based on a wave propagation experiment. A strong reflector, most likely the bedrock, was found at a depth of 17.3 m from the seabottom. The sediment consists of two layers with thicknesses 6.6 and 10.7 m. The mean velocities of these layers were estimated to 1425 and 1664 m/s. The velocity of the top sediment varies strongly by depth. At the seafloor the velocity is 1390 m/s, while it could be as large as 1575 m/s at the interface with the deep sediment. The details of the velocity profile are uncertain, and the linear profile in Fig.2.1 is free handed. The density and attenuation of the top sediment were estimated to $1500 kg/m^3$ and $0.15 dB/\lambda$, and of the bottom one to $1700 kg/m^3$ and $0.10 dB/\lambda$.

2.4 An example of almost horizontal rays

The sound speed profile of the water in Sec. 2.3 decreases from 1496 m/s at the surface to 1444 m/s at the bottom. The rate of decrease is largest at the thermocline at a depth of 10 m. The influence of the downward refracting profile is particularly strong when the source is located at the thermocline and radiating horizontally. This situation is depicted in Fig. 2.2. As can be seen, the ray dives into the sediment already at a range of 100 m, where a reflected and a transmitted wave emerge. Because of the the low impedance contrast at the water/sediment surface, most of the energy is transmitted into the bottom. It is made clear by drawing the ray paths with a line width proportional to intensity along the ray. The strong velocity gradient of the top sediment makes the ray turn before reaching the deep sediment. Most of the energy passes through the top sediment before returning to the water at the range 150 m.

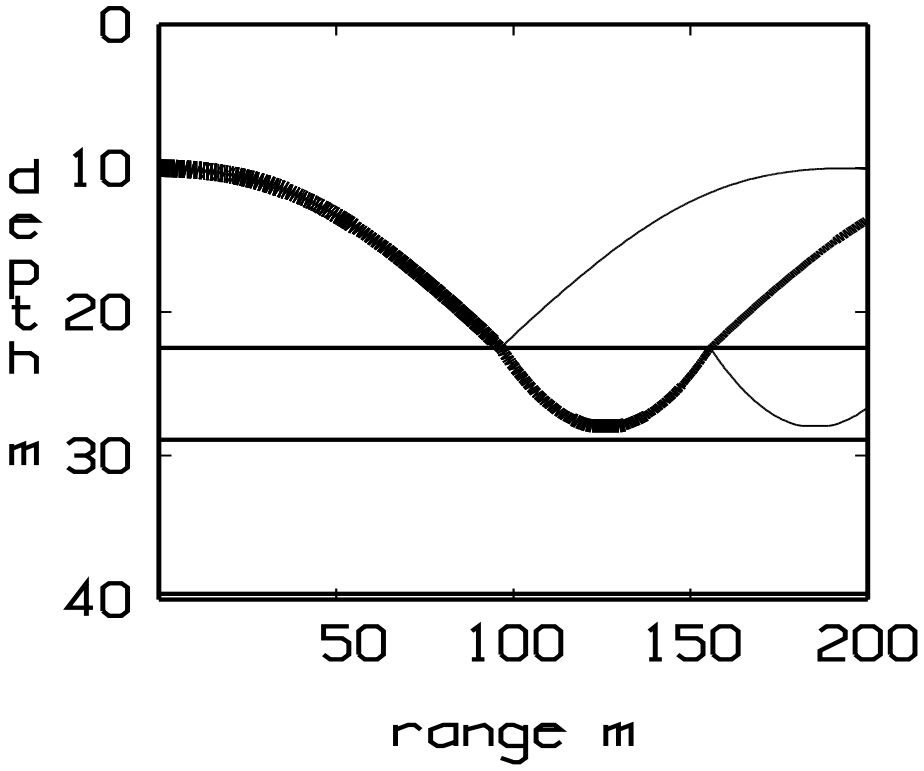

Figure 2.2: *This ray diagram illustrates refraction and reflection/transmission at a horizontal interface. The ray paths have been drawn with a line thickness proportional to intensity.*

2.5 An example of almost vertical rays

Figure 2.3 shows a ray diagram in which waves travel almost vertically. At a receiver in the water quite close to the source in range, the strongest return comes from a reflection at the bedrock interface some $18m$ down from the seabottom. Refraction effects are weak for near vertical propagation, and straight rays would be good enough.

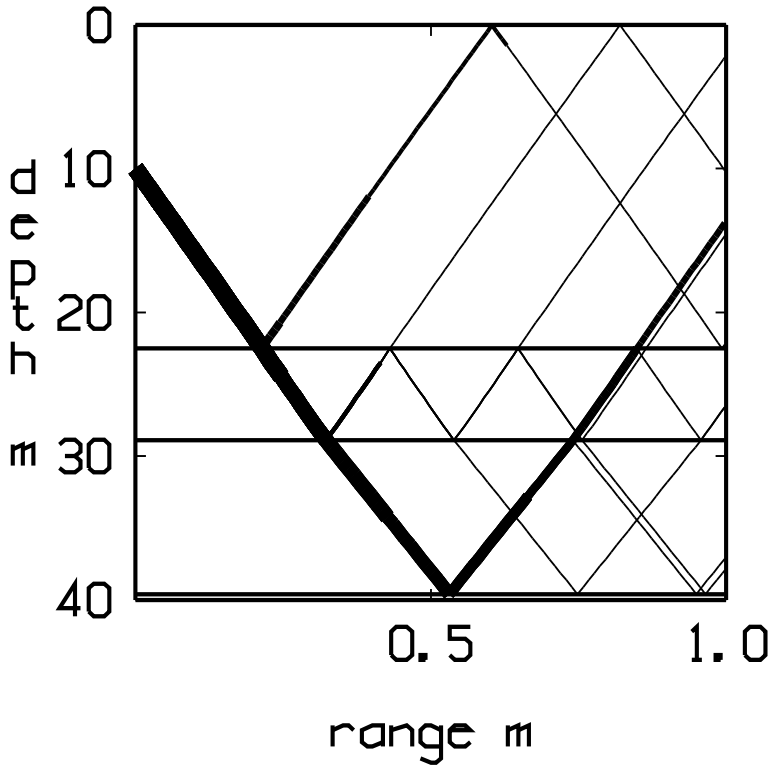

Figure 2.3: *This ray diagram should be compared with the previous one. It illustrates that refraction effects vary considerably depending on the direction of the wave in relation to the gradient of the velocity. Note that the horizontal scale is only* $1m$.

2.6 An example of eigenrays

The above pictures show how sound is propagated from a source which radiates in a single direction. A ray represents a whole ray tube in which acoustic energy is transmitted away from the source. To represent a real source a great number of rays is needed. However, computing a fan of rays does not directly provide an answer to the basic question in acoustic modeling, that is, to determine the response at the receiver for a given source and a given environment. For this purpose eigenrays are more useful than a bundle of rays. An eigenray is a ray path that joins two given points. In layered media there is an infinite number of eigenrays joining two given points. Figure 2.4 shows five eigenrays between a source and a receiver.

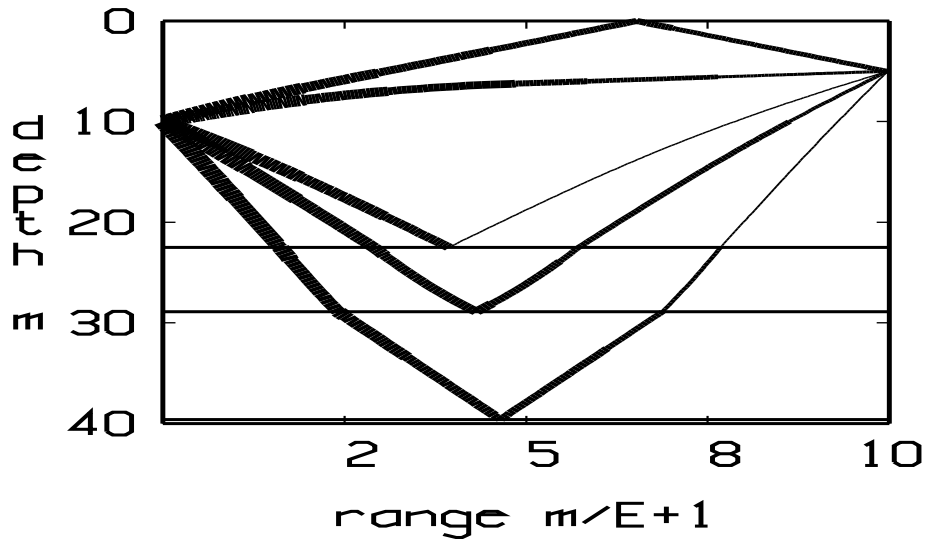

Figure 2.4: *This ray diagram shows five eigenrays between a source and a receiver.*

The most important parameters of each ray are listed in Table 1.1.

No	Time,ms	TL	TLgeo	TLref	TLabs	Angle	ray id
1	67.07	45.3	45.3	0	0	-7.54	-1
2	67.66	41.1	41.1	0	0	-11.05	-11
3	71.23	61.9	38.7	23.2	0	14.57	11
4	74.55	43.3	39.6	0.5	3.2	21.05	1221
5	77.74	49.2	43.2	0.9	5.1	36.48	123321

Table 1.1. *Each ray is tabulated with arrival time, total transmission loss (dB), losses due to geometrical spread, interfaces and absorption. The departure angle at the source and layers traversed by the ray are also listed.*

Columns 2 and 3 show the travel time and transmission loss (TL) at the end of the ray. TL is the sum of three terms: the geometrical spread (TLgeo), losses due to reflection/transmission at interfaces (TLref) and absorption (TLabs). TLabs is the only loss term that depends on the frequency. In the present case the frequency is set to 1 kHz. The grazing angle of departure (Angle) at the source is also listed. A minus sign indicates that the ray is directed towards the sea surface. The last column is a ray identifier. It is a sequence of digits, which indicates the layers being traversed by the ray.

Supplemented by information of the phase, this table makes it possible to compute the sound field at the receiver for both time-harmonic and transient sources. It is done by summing the sound fields from each ray making use of both amplitudes and phases in the frequency domain. Pulse propagation is accomplished by Fourier synthesis. At short separation distances only a few rays are needed, because the amplitude of multireflected rays decays rapidly as the angles get steeper.

3 The geoacoustic profile

Several assumptions of the geoacoustic profile is made in the model forming the basis of RAYLAB. First, it is asumed that the sea and the sub-bottom layers are horizontally stratified (range-independence). Second, we assume that the acoustics of the seabed is the same as for a fluid medium. It means that the influence of shear elasticity is neglected. In return these simplifications substantially reduce the computional effort as will be explained later on.

3.1 The acoustic wave equation

Sound transmission in a fluid medium like air or water is governed by the acoustic wave equation

$$\frac{1}{c^2}\frac{\partial^2 p}{\partial t^2} = \rho\nabla(\frac{1}{\rho}\nabla p) + f, \tag{3.1}$$

where

$p =$ $p(\mathbf{x}, t)$, acoustic pressure $[Pa]$,

$c =$ $c(\mathbf{x})$, speed of sound $[m/s]$,

$\rho =$ $\rho(\mathbf{x})$, density $[kg/m^3]$,

$f =$ $f(\mathbf{x}, t)$, acoustic sources $[Pa/m^2]$,

$\mathbf{x} =$ (x, y, z), cartesian coordinates, $[m]$.

3.2 Environmental assumptions

We consider the wave equation in a horizontally stratified marine environment of seawater and a plane layered bottom, see Fig. 3.1.

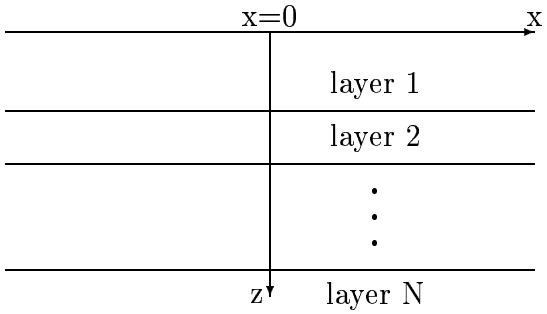

Figure 3.1: *A sea environment with N plane layers.*

The deepest layer is assumed to be a half-infinite stratum of bedrock with constant density and speed of sound.

The sea surface at $z = 0$ is assumed to be ideally flat and sound soft. Mathematically this condition is expressed by the pressure release condition

$$p(x, y, 0, t) = 0, \quad -\infty < x, y < \infty.$$

Physically it implies that the sea surface is perfectly reflective, and all sound transmission from the water into the air space or vice versa is neglected.

The absence of range variations implies that the speed of sound and density may depend only on the depth coordinate z. In RAYLAB they are specified in each layer as two-column tables of depth coordinates and velocity and density values. The profiles are made continuous within each layer by a piecewise linear approximation based on tabular values. In general there are jumps in velocities and densities at layer boundaries.

Due to media discontinuities at layer boundaries there is one wave equation (3.1) in each layer. The solutions are tied at a layer interface z_b by the boundary conditons

$$\begin{aligned} p(x, y, z_b-, t) &= p(x, y, z_b+, t), \\ \frac{1}{\rho}\frac{\partial p}{\partial z}(z_b-) &= \frac{1}{\rho}\frac{\partial p}{\partial z}(z_b+) \end{aligned} \tag{3.2}$$

for $-\infty < x, y < \infty, \quad t \geq 0$. Here $z_b\pm$ denote the limiting values on either side of the boundary. Physically the conditions (3.2) imply that the pressure and normal particle velocity are continuous at layer boundaries.

For pulse propagation we assume that the wave equation (3.1) is is to be solved for $t \geq 0$ with the initial conditions

$$p(\mathbf{x}, 0) = \frac{\partial p(\mathbf{x}, 0)}{\partial t} = 0. \tag{3.3}$$

It means that the simulations start with quiescent conditions.

The acoustic source, represented by the forcing function f in the wave equation (3.1), is assumed to be a simple monopole

$$f(\mathbf{x}, t) = s(t)\delta(x - x_s)\delta(y - y_s)\delta(z - z_s) \tag{3.4}$$

where $\mathbf{x}_s$ is the source position and $s(t)$ is a time-dependent amplitude function.

Time-harmonic sources are of particular importance in all aspects of wave propagation. In the time-harmonic case it is preferable to introduce a complex pressure u and a complex source amplitude $\hat{s}$ according to

$$\begin{aligned} p(\mathbf{x}, t) &= Re(u(\mathbf{x})e^{-i\omega t}), \\ s(t) &= Re(\hat{s}e^{-i\omega t}), \\ \omega &= 2\pi f, \quad f \text{ frequency in Hz.} \end{aligned}$$

By substituting the complex, time-harmonic quantities into the wave equation we obtain the Helmholtz equation

$$\rho\nabla(\frac{1}{\rho}\nabla u) + k^2(\mathbf{x})u = -\delta(z - z_s)\delta(x)\delta(y), \tag{3.5}$$

where for simplicity we have put $\hat{s} = 1$ and $x_s = y_s = 0$. The wavenumber k $[m^{-1}]$

$$k(z) = \frac{\omega}{c(z)} \tag{3.6}$$

depends only on the depth coordinate in the horizontally layered case. It is common to define a local wavelength λ by

$$\lambda(z) = \frac{c}{f} = \frac{2\pi}{k(z)}.$$

In an infinite and homogeneous medium (whole-space), the solution to the Helmholtz equation (3.5) is given by

$$\begin{aligned} u(\mathbf{x}) &= \frac{1}{4\pi R} e^{ikR}, \\ R &= (x^2 + y^2 + (z - z_s)^2)^{\frac{1}{2}}. \end{aligned} \tag{3.7}$$

The solution (3.7) is a spherically symmetric wave, whose amplitude decays by the inverse of the distance to the source.

Wave attenuation due to absorption is introduced by adding an imaginary part to the wavenumber according to

$$k = \frac{\omega}{c(z)}(1 + i\frac{\alpha(z)\ln 10}{40\pi}), \tag{3.8}$$

where the absorption parameter $\alpha(z)$ is expressed in dB/λ. By using the complex k (3.8) in the fundamental solution (3.7), it is verified that the decay due to absorption is α dB in one wavelength.

The sound field from an omnidirectional point source in a range-independent medium has cylindrical symmetry with respect to a z-axis through the source. The Helmholtz equation in cylindrical coordinates (r, ϕ, z) for solutions $u(r, z)$ with azimuthal symmetry is given by

$$\frac{1}{r}\frac{\partial}{\partial r}(r\frac{\partial u}{\partial r}) + \rho\frac{\partial}{\partial z}(\frac{1}{\rho}\frac{\partial u}{\partial z}) + k^2(z)u = -\frac{\delta(r)}{2\pi r}\delta(z - z_s). \tag{3.9}$$

The azimuthal symmetry implies that the solution needs to be computed only in two coordinates (r, z), or equivalently, in a vertical plane through the cylinder axis. This symmetry leads to huge computational savings.

All computations in RAYLAB are based on the two-dimensional Helmholtz equation (3.9). However, from a user's perspective, sources and receivers may be located freely in a three-dimensional coordinate system suitably defined by the user. Computationally, the total field is obtained by a summation over sources, each of which is radiating an azimuthally symmetric field.

4 The ray model

The ray approach is said to be a high frequency approximation, although this phrase is too vague, because the frequency is a dimensional quantity $[s^{-1}]$. For example, in a whole-space the ray solution is identical to the fundamental solution (3.7) independently of the frequency. A more relevant condition is that the variations of the media parameters or the geometry should be small over one wavelength. If the media changes gently, higher frequencies means smaller wavelengths and ultimately this condition is fulfilled. However, when the spatial scale of media variations is comparable to, or smaller than the wavelength, the notion of wavefront is lost and sound is spread in different directions, the extent of which depends on the frequency. The most well-known diffraction phenomenon is the bending of low-frequency sound around obstacles. The most severe shortcoming of the ray model is the absence of diffraction. To cope with this defiency a geometrical theory of diffraction was developed in [2]. More recent attempts to capture frequency dependent features are complex ray theory [3] and Gaussian beams [4]. RAYLAB is an implementation of the classical ray model without extensions. We proceed with an account of how the ray theory in [5] has been applied. In addition, the derivations include density profiles.

4.1 Fundamental equations in ray theory

The basic ray equations are obtained by seeking a solution in terms of a high frequency asymptotic expansion

$$u(r,z) = e^{i\omega\tau(r,z)} \sum_{n=0}^{\infty} A_n(r,z)(i\omega)^{-n}. \tag{4.1}$$

The expansion (4.1) is substituted into the Helmholtz equation (3.9) (without the source term), and the sequence of coefficients of different powers of ω are collected and set to zero. The first term is the eikonal equation

$$(\frac{\partial\tau}{\partial r})^2 + (\frac{\partial\tau}{\partial z})^2 = \frac{1}{c^2(z)} \tag{4.2}$$

for the phase τ (apart from the multiplying factor ω). The next term is the transport equation

$$2(\frac{\partial\tau}{\partial r}\frac{\partial A_0}{\partial r} + \frac{\partial\tau}{\partial z}\frac{\partial A_0}{\partial z}) + \left(\frac{1}{r}\frac{\partial}{\partial r}(r\frac{\partial\tau}{\partial r}) + \rho\frac{\partial}{\partial z}(\frac{1}{\rho}\frac{\partial\tau}{\partial z})\right) A_0 = 0. \tag{4.3}$$

The subsequent terms are corrections to the amplitude, and they are omitted since their importance diminish as $\omega \to \infty$. As opposed to the amplitude, no further corrections in powers of ω^{-1} appear for the phase. This fact indicates that the phase, or equivalently, the travel time is very accurate in ray theory even at low frequencies. We also see from the eikonal equation (4.2), that neither the density nor its variation affect the phase.

The equations (4.2) and (4.3) are solved in succession. Once the phase τ has been found from the eikonal equation, it is substituted into the transport equation, which then becomes a linear partial differential equation for the leading term of the amplitude.

4.2 Solving the eikonal equation

4.2.1 Analytic formulas

The eikonal equation is a nonlinear partial differential equation, which can be solved by the method of characteristics [6]. The essence of this approach is to keep track of the wavefronts, which are curves of constant phase τ. The ray trajectories are curves orthogonal to the wavefronts. It means that the tangent vector of the ray path is parallel to the gradient vector $\nabla\tau$. Let $(r(s), z(s))$ be a parametrization of the ray, where s is the arclength. Then the above condition implies that

$$\frac{dr}{ds} = c\frac{\partial\tau}{\partial r}, \quad \frac{dz}{ds} = c\frac{\partial\tau}{\partial z}. \tag{4.4}$$

The normalization factor c is a direct consequence of the eikonal equation (4.2) and the unit length of the tangent vector. Looking at the ray ansatz (4.1), it is natural to introduce a local wave vector $\mathbf{k}$ as

$$\mathbf{k} = (k_r, k_z) = (\frac{\partial\tau}{\partial r}, \frac{\partial\tau}{\partial z}). \tag{4.5}$$

From the eikonal equation it follows that

$$k = |\mathbf{k}| = (k_r^2 + k_z^2)^{\frac{1}{2}} = \frac{1}{c(z)}, \tag{4.6}$$

which is consistent with the wave number k of the Helmholtz equation (3.9). Here and subsequently, the wave number is only for the frequency $\omega = 1$. It is a good convention in dealing with the ray equations, because they are independent of the frequency. Only in the very end, the phase including an imaginary part due to absorption needs to be multiplied by the actual frequency ω.

Next we consider waves propagating outwards from the source at $(0, z_s)$. Then

$$k_r \geq 0, \quad \pm k_z = \pm\sqrt{k^2(z) - k_r^2}, \tag{4.7}$$

where the sign in front of $k_z \geq 0$ indicate the vertical direction of the wave. The equations (4.4) for the ray trajectory can now be written as

$$\frac{dr}{ds} = ck_r, \quad \frac{dz}{ds} = \pm c\sqrt{k^2(z) - k_r^2}. \tag{4.8}$$

To be able to solve these equations, an additional equation is needed for k_r in terms of c is needed. It is obtained by differentiation of k_r along the ray path:

$$\begin{aligned}
\frac{dk_r}{ds} &= \frac{d}{ds}(\frac{\partial\tau}{\partial r}) = \frac{\partial^2\tau}{\partial r^2}\frac{dr}{ds} + \frac{\partial^2\tau}{\partial r\partial z}\frac{dz}{ds} \\
&= c(\frac{\partial^2\tau}{\partial r^2}\frac{\partial\tau}{\partial r} + \frac{\partial^2\tau}{\partial r\partial z}\frac{\partial\tau}{\partial z}) \\
&= \frac{1}{2}c\frac{\partial}{\partial r}\left((\frac{\partial\tau}{\partial r})^2 + (\frac{\partial\tau}{\partial z})^2\right) \\
&= \frac{1}{2}\frac{\partial}{\partial r}\frac{1}{c^2} = 0.
\end{aligned} \tag{4.9}$$

The last equality follows from the assumption of range independence. Therefore the horizontal wave number is a constant along the entire ray path. This result can also be derived directly from the Helmholtz equation (3.9) using the method of separation of variables. The invariance of k_r also holds across layer boundaries, that is, the incident and transmitted waves have the same k_r. It is an alternative way of stating Snell's law, and it is also called the Snell invariant. It is the key to many computational simplifications.

For a point source at $(0, z_s)$ the pair (4.8) of ordinary differential equations is solved for $s \geq 0$ with initial conditions equal to

$$x(0) = 0, \quad z(0) = z_s \tag{4.10}$$

and a prescribed value of

$$k_r, \quad 0 \leq k_r \leq \frac{1}{c(z_s)} = k(z_s) \tag{4.11}$$

and sign of k_z.

The grazing take-off angle θ_s of the ray at the source is given by

$$\theta_s = \pm cos^{-1}(\frac{k_r}{k(z_s)}), \quad -\frac{\pi}{2} \leq \theta_s \leq \frac{\pi}{2} \tag{4.12}$$

with positive angles for rays directed towards the bottom. The angle θ_s is not used as a ray parameter in RAYLAB. It more convenient to use k_r and the sign of k_z, simply because k_r is not related to the position of the source.

In practice the ray equations (4.8) are reduced to one equation by expressing the radial distance of the ray path as a function of the depth coordinate according to

$$\frac{dr}{dz} = \frac{k_r}{\pm\sqrt{k^2(z) - k_r^2}}, \quad k^2(z) = \frac{1}{c^2(z)}. \tag{4.13}$$

The equation (4.13) is solved piece by piece with one sign at a time corresponding to waves traveling down (+) or up (-). The ray is traced until it encounters a turning point (r_t, z_t) defined by

$$k^2(z_t) - k_r^2 = 0, \tag{4.14}$$

or intersects a layer boundary at (r_b, z_b). At a turning point the ray path is horizontal with $k_z = 0$. After the turning point three cases may be distinguished depending on

$$i) \quad c'(z_t) \neq 0, \quad ii) \quad c'(z_t) = 0, \quad iii) \quad \text{nonexistant} \quad c'(z_t). \tag{4.15}$$

In the first case, the ray direction is reversed after passage of (r_t, z_t). If $c^{'}(z_t) = 0$, the ray exhibits a higher order contact with the horizontal line $z = z_t$, after which it may continue up or down depending on the sign of the first nonzero derivative of c at z_t. If c is nondifferentiable at the turning point, the ray may split into a multitude of rays. In RAYLAB the first case is always assumed to hold. It is a practical means of avoiding any pecularities of the sound speed profile around the turning point. The piecewise linear approximation of data in RAYLAB hardly admits further sophistication.

When a ray intercepts a layer boundary at (r_b, z_b), a choice is made whether to continue with a backreflected or a transmitted wave. In RAYLAB this choice is done prior to the ray tracing by specifying layers to be traversed. In any case, a new piece of the ray is started at (r_b, z_b). For a backreflected way, the sign of k_z is changed, while transmission requires a new k_z according to

$$\pm k_z = \pm\sqrt{k^2(z_b\pm) - k_r^2} \tag{4.16}$$

provided that $k_r < k(z_b\pm)$. Radiation at the critical angle, corresponding to $k_r = k(z_b\pm)$, is not within the realm of classical ray theory.

4.2.2 Numerical formulas

For a general sound speed profile, the equation (4.13) must be solved numerically by a Runge-Kutta method for example. However, explicit solutions do exist for linear profiles in c or k^2 [5]. The latter case is adopted in RAYLAB. In each layer a piecewise linear k^2-profile is formed using the same sublayer points as the input sound speed profile, that is,

$$(z_n, k^2(z_n)) = (z_n, \frac{1}{c^2(z_n)})$$

where n ranges over the number of points of the profile. Thus if $z \in [z_n, z_{n+1}]$, the linear approximation

$$k^2(z) = k^2(z_n) + b_n(z - z_n),$$

where

$$b_n = \frac{k^2(z_{n+1}) - k^2(z_n)}{z_{n+1} - z_n} \tag{4.17}$$

is employed. With this approximation, the equation (4.13) can be integrated analytically. The result is

$$\begin{aligned} r(z_b) &= r(z_a) + \frac{2k_r|z_b - z_a|}{k_z(z_b) + k_z(z_a)} \\ k_z(z) &= \sqrt{k^2(z_n) + b_n(z - z_n) - k_r^2}, \end{aligned} \tag{4.18}$$

where z_a, z_b are any two points such that

$$z_n \le z_a \le z_b \le z_{n+1}, \quad \text{downgoing ray},$$

or

$$z_n \le z_b \le z_a \le z_{n+1}, \quad \text{upgoing ray}.$$

If a turning point is encountered, then either $k_z(z_a)$ or $k_z(z_b)$ is zero. Such a point is the starting point of a new piece of the ray in which the depth coordinate is traversed in the opposite direction.

If the ray traverses the entire layer, the formula (4.13) is applied sublayer by sublayer, in which z_a and z_b are the boundary points of the sublayers. It implies that computational cost increases by the number of points of the sound velocity profiles of the water and sediments.

If the ray stays within the same layer, it will cycle up and down between two extremal points in depth, which are the layer boundaries and/or turning points.
The phase τ along the ray trajectory satisfies the equation

$$\frac{d\tau}{ds} = \frac{dr}{ds}\frac{d\tau}{dr} + \frac{dz}{ds}\frac{d\tau}{dz} = c((\frac{\partial\tau}{\partial r})^2 + (\frac{\partial\tau}{\partial z})^2) = \frac{1}{c(z)} = k(z). \tag{4.19}$$

It implies that τ is the travel time along the path. Using

$$ds = \frac{k(z)}{k_z(z)}dz$$

and the linear approximation of k^2, analytic integration gives

$$\begin{aligned} \tau(r_b, z_b) &= \tau(r_a, z_a) + \delta\tau \\ \delta\tau &= \frac{2}{3}|z_b - z_a|\frac{k^2(z_b) + k^2(z_a) + k_z(z_b)k_z(z_a) + k_r^2}{k_z(z_b) + k_z(z_a)} \end{aligned} \tag{4.20}$$

for the points (r_a, z_a) and (r_b, z_b) on the ray (4.18).
In the ray representation (4.1), the phase $\omega\tau$ is simply obtained by multiplying the travel time (4.20) by ω. Media absorption is modeled by adding an imaginary part to the phase. The increments of the real and imaginary parts of the phase between two points (r_a, z_a) and (r_b, z_b) on the path (4.18) is computed as

$$\begin{aligned} Re(phase) &= \omega\delta\tau \\ Im(phase) &= \frac{\ln 10}{40\pi}\frac{\alpha(z_b) + \alpha(z_a)}{2}\omega\delta\tau, \end{aligned} \tag{4.21}$$

where $\delta\tau$ is given by (4.20), and $\alpha(z)$ is the absorption profile.
Additional phase changes due to reflection/transmission at layer boundaries and intercepts with caustics will be discussed later on.

4.3 Solving the transport equation

4.3.1 Analytic derivations

The amplitude associated with each ray is determined by the transport equation (4.3). It can be solved analytically along the ray path. Next we briefly review the derivation given in [5] but adding density variations.
The first part of the transport equation can be written as

$$2(\frac{\partial\tau}{\partial r}\frac{\partial A_0}{\partial r} + \frac{\partial\tau}{\partial z}\frac{\partial A_0}{\partial z}) = \frac{2}{c(z(s))}\frac{dA_0}{ds} \tag{4.22}$$

using the equations (4.4) for the ray path. In order to evaluate the last term of the transport on the ray path, consider the Jacobian of the transformation from the ray coordinates (s, θ_s, ϕ_s) to the cylindrical coordinates (r, z, ϕ_s), where the subscript s

refers to conditions at the source position. In case of azimuthal symmetry the Jacobian is given by

$$J = r(\frac{\partial r}{\partial s}\frac{\partial z}{\partial \theta_s} - \frac{\partial z}{\partial s}\frac{\partial r}{\partial \theta_s}). \tag{4.23}$$

By differentiation of the Jacobian along the ray path, it can be shown that

$$\frac{\rho}{J}\frac{d}{ds}(\frac{J}{\rho c}) = \frac{1}{r}\frac{\partial}{\partial r}(r\frac{\partial \tau}{\partial r}) + \rho\frac{\partial}{\partial z}(\frac{1}{\rho}\frac{\partial \tau}{\partial z}). \tag{4.24}$$

Using the identities in (4.22) and (4.24) the transport equation can be written as an ordinary differential equation along the ray path:

$$\frac{2}{c}\frac{dA_0}{ds} + \frac{\rho}{J}\frac{d}{ds}(\frac{J}{\rho c})A_0(s) = 0. \tag{4.25}$$

By multiplying this equation by $JA_0\rho^{-1}$, it can be written as

$$\frac{d}{ds}(A_0^2\frac{1}{\rho c}J) = 0. \tag{4.26}$$

It means that

$$\left(A_0^2\frac{1}{\rho c}J\right)(s) \equiv \left(A_0^2\frac{1}{\rho c}J\right)(0), \quad s \geq 0, \tag{4.27}$$

where the constant on the right is evaluated at the source. It is done such that the ray solution is identical to the whole-space solution (4.22) in the vicinity of the source.

The physical interpretation of the identity (4.27) is that the energy flux along the ray is invariant. The amplitude squared divided by the impedance ρc is the intensity, while J is a geometrical factor of dimension $[m^2]$. When J is multiplied by $d\theta_s$ it signifies the transversal area swept out by the end points of two $d\theta_s$-separated rays as they are rotated around the cylinder axis.

4.3.2 Computing the amplitude

The evaluation of the derivatives of the Jacobian (4.23) on the ray path requires some footwork. Let $\theta(s)$ denote the grazing angle of the ray path given by

$$\frac{dr}{ds} = \cos\theta(s), \quad \frac{dz}{ds} = \sin\theta(s).$$

The derivatives with respect to θ_s express the rate of variation along the wavefront. By inspection of the ray geometry we find that

$$\begin{aligned} \frac{\partial z}{\partial \theta_s} &= -\frac{\cos\theta}{\sin\theta}\frac{\partial r}{\partial \theta_s}|_{s=const}, \\ \frac{\partial r}{\partial \theta_s}|_{s=const} &= \sin^2\theta\frac{\partial r}{\partial \theta_s}|_{z=const}. \end{aligned} \tag{4.28}$$

Replacing the take-off angle θ_s by k_r as ray parameter, implies that

$$\frac{\partial r}{\partial \theta_s} = \frac{\partial r}{\partial k_r}\frac{dk_r}{d\theta_s} = -k(z_s)\sin\theta_s\frac{\partial r}{\partial k_r}.$$

Subsequently, the derivative of the range of the ray with respect to k_r is always understood to be evaluated for a fixed depth coordinate.

When the above relations are substituted into the Jacobian (4.23), we obtain

$$J = r k_s \sin\theta_s \sin\theta \frac{\partial r}{\partial k_r}.$$

In the code the energy invariant (4.27) is applied piece by piece like the ray tracing formula (4.18). For two successive points (r_a, z_a) and (r_b, z_b) on the ray, it implies that

$$A_b^2 = A_a^2 \frac{\rho_b}{\rho_a} \frac{r_a}{r_b} \frac{k_z(z_a)}{k_z(z_b)} \frac{|\frac{\partial r}{\partial k_r}|_a}{|\frac{\partial r}{\partial k_r}|_b}, \tag{4.29}$$

where

$$k_z = \sqrt{k^2(z) - k_r^2}, \quad \sin\theta = \pm k_z/k.$$

For a point source at $(0, z_s)$, the formula (4.29) is initialized by putting

$$A_a = \frac{1}{\cos\theta_s}, \quad r_a = 1, \quad \rho_a = \rho_s, \quad k_z \frac{\partial r}{\partial k_r}|_a = \frac{1}{k_r k_z(z_s)},$$

which corresponds to the whole-space solution (3.7) apart from the factor 4π.

The formula (4.29) can also be continued after intersections with layer boundaries by multiplying the amplitude by the magnitude of the reflection/transmission coefficient according to plane wave analysis. The phase angle of a complex coefficient is added to the accumulated sum of phase contributions along the path.

4.3.3 Evaluating the range derivative

It remains to evaluate the range derivative in (4.29). It warrants special attention, because the range derivative may become infinite (turning points) or zero (caustics). Consider the ray tracing formula (4.18) for a downgoing wave in a sublayer $[z_n, z_{n+1}]$, that is,

$$r(z) = r(z_n) + \frac{2k_r(z - z_n)}{k_z(z) + k_z(z_n)}, \tag{4.30}$$

where

$$k_z(z) = \sqrt{k^2(z_n) + b_n(z - z_n) - k_r^2}, \quad k(z_n) = \frac{1}{c(z_n)}.$$

Differentiating (4.30) with respect to k_r gives

$$\begin{aligned} \frac{dr(z)}{dk_r} &= \frac{dr(z_n)}{dk_r} + \delta\frac{dr}{dk_r} \\ \delta\frac{dr}{dk_r} &= \frac{2(z - z_n)}{k_z(z) + k_z(z_n)} \left(1 + \frac{k_r^2}{k_z(z)k_z(z_n)}\right) \end{aligned} \tag{4.31}$$

provided that $k_z > 0$ in $[z_n, z]$. This formula is used to update the range derivative within a sublayer.

If

$$k_r < min_{0 \le z \le z_B} k(z),$$

where z_B is the depth of the half-infinite bottom, then the range derivative remains positive over the entire path, and $r(z, k_r)$ is an increasing function of k_r for any depth point z.

If $b_n < 0$, there may be a turning point z_t, $z_n < z_t < z_{n+1)}$, defined by

$$k_z(z_t) = \sqrt{k^2(z_n) + b_n(z_t - z_n) - k_r^2} = \sqrt{k^2(z_t) - k_r^2} = 0.$$

Then it follows from (4.31), that

$$\delta \frac{dr}{dk_r} \to \infty \text{ as } z \to z_t. \tag{4.32}$$

However, when the range derivative is multiplied by k_z in the amplitude formula (4.29), there is a limiting value

$$k_z(z_t) \frac{dr(z_t)}{dk_r} = (z_t - z_n) \frac{k_r^2}{k_z^2(z_n)}.$$

It implies that the amplitude is well defined at the turning point. After reversal of direction at the turning point, the ray consists of two pieces:

$$\begin{aligned} r(z_t) &= r(z_n) + \frac{2k_r(z - z_n)}{k_z(z_n)}, \\ r(z) &= r(z_t) + \frac{2k_r(z_t - z)}{k_z(z)}. \end{aligned} \tag{4.33}$$

Differentiating with respect to k_r give

$$\begin{aligned} \delta \frac{dr}{dk_r}|_d &= \frac{2(z_t - z_n)}{k_z(z_n)} \left(1 + \frac{k_r^2}{k_z^2(z_n)}\right) + \frac{2k_r}{k_z(z_n)} \frac{dz_t}{dk_r} \\ \delta \frac{dr}{dk_r}|_u &= \frac{2(z_t - z)}{k_z(z)} \left(1 + \frac{k_r^2}{k_z^2(z)}\right) + \frac{2k_r}{k_z(z)} \frac{dz_t}{dk_r} \end{aligned} \tag{4.34}$$

where the subindices d, u refer to waves down and up. Since z_t satifies the equation

$$k^2(z_n) + b_n(z_t - z_n) - k_r^2 = 0$$

we obtain

$$\frac{dz_t}{dk_r} = \frac{2k_r}{b_n},$$

where b_n is the gradient (4.17) of k^2 in $[z_n, z_{n+1}]$. As a result we obtain

$$\begin{aligned} \delta \frac{dr}{dk_r}|_d + \delta \frac{dr}{dk_r}|_u = &\frac{2(z_t - z_n)}{k_z(z_n)} \left(1 + \frac{k_r^2}{k_z^2(z_n)}\right) + \frac{4k_r^2}{k_z(z_n) b_n} \\ &+ \frac{2}{k_z(z)} \left((z_t - z) + \frac{k_r^2}{b_n}\right), \end{aligned} \tag{4.35}$$

where also the relation

$$k_z^2(z) = b_n(z - z_t), \quad b_n < 0,$$

has been used. When multipling by $k_z(z)$, it can be verified that the ray amplitude assumes the same limiting values on both sides of the turning point.

The dominant term in (4.35) as $z \to z_t$ is the last one, for which

$$\frac{2k_r^2}{k_z(z)b_n} \to -\infty \quad \text{as} \quad z \to z_t.$$

However, the expression (4.35) for the increment of the range derivative is increasing as z decreases, and it may happen that it becomes zero at some point (r_c, z_c). The envelope of all points for which

$$\frac{dr(r_c, z_c)}{dk_r} = 0$$

for a bundle of rays is a caustic. On the caustic the ray amplitude is infinitely large. The caustic separates an insonified side from a shadow one. This boundary is sharp in ray acoustics, while in reality it is more or less diffuse depending on the frequency. A detailed study of both the sound field and the ray solution in the vicinity of caustics is presented in [7].

If the point $(r_b, z_b) = (r_c, z_c)$ would appear in the amplitude formula (4.29), it would cause a division by zero. Although a direct hit on the caustic is an unlikely event in numerical ray tracing, this situation should be guarded. It could be accomplished by a slight move of the sampling point on the ray path. With this reservation, the amplitude formula (4.29) can be applied both before and after the caustic.

It is well known that the wave undergoes a phase shift of $-\pi/2$ (time-advance) as it touches the caustic. It is dealt with by checking the sign changes of the range derivative.

5 Finding the eigenrays

5.1 The theoretical setup

For a given point source $(0, z_s)$ and receiver at (r_e, z_e), and a given ray type, the eigenray problem is to find all rays which connect the source and receiver. The direct ray is the ray which has been reflected at neither the sea surface nor the bottom, nor has it changed directions by the passage of a turning point. This ray is unique, if it exists. The next type is the ray that has changed directions once, either by a reflection or a turning refraction. It is called the surface (bottom) reflected or refracted ray. There may exist several refracted rays of the same type. In RAYLAB each type of ray is specified by a code of digits, where each digit corresponds to a single traversal of a layer, either up or down. For example, the rays just mentioned possess the codes ± 1, $+11$, -11. The plus sign implies that the ray is launched towards the bottom and minus is for upward directed rays from the source. The subsequent digits in the order left to right denote successive layer traversals, which may be incomplete if the ray direction is reversed at a turning point. The first digit, a '1' represents the ray piece from the source to the

sea surface of bottom or a turning point within the water. A similar remark holds for the last digit. A traversal of layer two, that is, the top sediment, is indicated by the digit 2. For example, the ray with the code -11221 is first reflected at the sea surface (or a turning point above the source), after which it returns to the sea bottom. It penetrates the top sediment, where its direction is reversed either by a turning point or a reflection at the interface with the next sediment. The last digit corresponds to the ray piece from the sea bottom to the receiver.

In RAYLAB the eigenray finding is made an entirely independent task for each choice of source, receiver and ray type. It also means that the computational cost is additive in terms of number of ray types and the number of combinations of sources and receivers.

The mathematical formulation of the eigenray problem is as follows. Find the horizontal wave numbers k_r, which satisfy the range equation

$$r(k_r, z_e) = r_e \tag{5.1}$$

where $r(k_r, z_e)$ is the range of the intersection point of the ray and the horizontal line $z = z_e$. In general there are several such intersection points along the ray path. The one being referred to is the intersection point after completion of all reversals of directions as specified by the ray type. In the sequel, we use the notation $r(k_r)$ for the range function in (5.1). It should be distinguished by the context from notation $r(z)$ which was used for the range of a single ray as function of depth.

The range $r(k_r)$ is computed by the formula (4.18) with $z_b = z_e$ and $z_a = z_n$ or $z_a = z_{n+1}$ depending on the arrival direction of the ray at the receiver. Prior to this, the ray has been traced through all layers, except the very last sublayer, as specified by the ray type. The range derivative dr/dk_r is evaluated by the formulas (4.31) or (4.35). The latter one is used for the passage of a turning point. The derivative is not defined at the turning point itself, where it changes from $+\infty$ to $-\infty$.

5.2 Solving the range equation

The general approach of solving the range equation (5.1) is to find k_r^L and k_r^R which bracket the range r_e, that is,

$$r(k_r^L) < r_e < r(k_r^R). \tag{5.2}$$

In addition it must be ensured that $r(k_r)$ is a continuous function between k_r^L and k_r^R. The conditions imply that there is at least one root k_r^*, that is,

$$r(k_r^*) = r_e \tag{5.3}$$

within the bracket (5.2). Once the bracket and the continuity condition have been established, it is easy to compute k_r^*. Since dr/dk_r is available, Newton's method can be applied. If it fails, it is backed by the method of bisection. However, due attention must be paid to the possibility of several roots within the bracket (5.2).

There are two major obstacles in finding a bracket (5.2). After the passage of a turning point, the ray path with $k_r = k_r^c$ may intersect a caustic at (r_c, z_c), where the range derivative vanishes. Now if $z_c = z_e$, and k_r^c, r_c are within the bracket (5.2), the range

function is not monotone when k_r spans the interval between k_r^L and k_r^R. In case there are several intersection points between the caustic and the horizontal line $z = z_e$, there may exist a number of solutions within the bracket (5.2).

The second major difficulty is the presence of discontinuity points of the range function $r(k_r)$. For example, consider two sublayers $[z_{n-1}, z_n]$ and $[z_n, z_{n+1}]$ with velocities $c_n > c_{n-1}$ and $c_n > c_{n+1}$ at the sampling points. Then a ray trace downwards will turn upwards before reaching z_n for $k_r = k_n - \epsilon$, while it continues downwards at z_n for $k_r = k_n + \epsilon$. It means that the ray path is discontinuous for $k_r = k_n$. Next we describe a device by which discontinuity points are excluded from the search domain of k_r. Similar ideas were persued in [8].

5.2.1 Partitioning the wave number space

We divide the search space of k_r^2 into a number of intervals, each of which is associated with a depth range:

$$\begin{aligned} k_{rj}^2 < & k_r^2 < k_{r,j+1}^2 \\ z_j < & z < z_{j+1}. \end{aligned} \tag{5.4}$$

The purpose of such a decomposition is to make sure that the range function $r(k_r)$ is continuous within each subdomain (5.4). Such a partition can be made prior to the ray tracing by a pure inspection of the sound speed profile. The discontinuity points of $r(k_r)$ will be the boundary points k_{rj} and $k_{r,j+1}$, which are simply excluded from the search domain (5.4) as indicated by strict inequalities. However, they may appear as interior points of other subdomains with a different depth range. The k_r^2-range constitutes a sound channel in which all rays are confined to the depth range (z_j, z_{j+1}). If z_s and/or z_e is outside this range, then the search domain can be disregarded, because there is no connecting ray between the source and receiver in this domain. The very first subdomain to be searched is given by

$$\begin{aligned} 0 < & k_r^2 < min_{0 \le z \le z_B} k^2(z) \\ 0 < & z < z_B, \end{aligned} \tag{5.5}$$

where z_B is the depth of the bottom of the deepest layer of the ray under consideration. The search domain (5.5) does not contain any turning points. It means that $r(k_r)$ is an increasing function of k_r. Therefore an eigenray, if it exists in this domain, is unique. Furthermore the influence of variations of the sound speed profile is weak because of fairly steep angles of propagation. A bracket can be found by using approximations by isovelocity layers. It can be done without ray tracing using analytic expressions for the range function. At the same time, the results of the isovelocity case determines whether there is an eigenray or not. The latter point is important, because all search domains are visited for all types of rays. In conclusion, whether there is an eigenray or not, the treatment of the domain (5.4) does not pose any difficulties. The boundary point $k_r = 0$ corresponds to a ray going straight down or up. Then the ray formula (4.18) is no longer applicable, and this case warrants a special treatment. To avoid this inconvenience, $k_r = 0$ is replaced by $k_r = \epsilon$, where the number ϵ is chosen by some

care so that the results become satisfactory. If the upper bound in (5.5) is assumed, the ray would become horizontal at a layer interface. The corresponding lateral wave is not part of the present ray model.

It remains to consider the remainder of the horizontal wave number space

$$min_{0\leq z\leq z_B} k^2(z) < k_r^2 < max_{0\leq z\leq z_B} k^2(z). \tag{5.6}$$

The domain is further restricted by the condition

$$k_r < min\{k_s, k_e\}, \tag{5.7}$$

since complex vertical wavenumbers (evanescent waves) are not allowed in classical ray theory.

The aim of dividing the domain (5.6) into subdomains is to avoid ambiguities when $k_z = 0$ at a sublayer boundary point. Such a point has a special significance because the sound speed profile is translated into a piecewise linear profile in $k^2(z)$ by putting $k_n^2 = 1/c_n^2$ from tabular values of the velocity. The profiles of each layer are concatenated into a single profile over the entire depth using double points at layer boundaries to signify jumps in velocity. This is the representation being referred to by the notation $k^2(z)$.

The general approach to create the desired decomposition is to let a vertical ruler slide from right to left over the entire $k^2(z)$- profile. It is stopped when a sound channel, in the following called a well, can be identified. Furthermore, rays in the well are not allowed to escape to a nearby well. The scheme to contain rays using separators in k_r space is made clear by the following example. Consider a section $n-1, n, n+1, .., n+m+1$ of the profile for which

$$\begin{aligned} k_n^2 \leq k_{n-1}^2, \quad k_{n+m+1}^2 \leq k_n^2 < k_{n+m}^2, \\ k_n^2 < k_{n+1}^2 < ... < k_{n+l}^2, \\ k_{n+m+1}^2 < k_{n+m}^2 < .... < k_{n+l}^2, \end{aligned} \tag{5.8}$$

see Fig. 5.1.

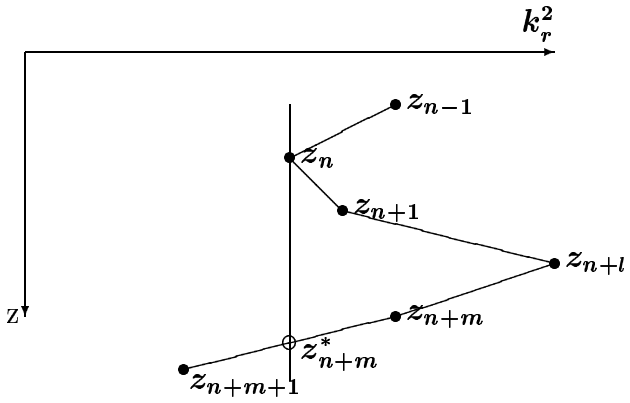

Figure 5.1: *The detachment of a well in k_r^2-space.*

The speed of sound has a local minimum at the bottom point (z_{n+l}, k^2_{n+l}) of the well. A subdomain of the type (5.4) is now formed by

$$\begin{aligned} &k_n^2 < k_r^2 < k_{r,n+l}^2 \\ &z_n < z < z^*_{n+m}, \quad z^*_{n+m} = z_{n+m} + \frac{z_{n+m+1} - z_{n+m}}{k^2_{n+m+1} - k^2_{n+m}}(k_n^2 - k^2_{n+m}) \end{aligned} \tag{5.9}$$

The vertical cut at k_n^2 prevents rays from escaping out of it once in there. Mathematically it implies that the range function is continuous within the domain (5.9). This domain need not be searched unless both z_s and z_e belong to the depth range in (5.9). A new $k^2(z)$-profile, called the ghost profile, is now created by moving all points $n+1, .., n+m$ to the vertical line between the endpoints in (5.9), that is, their k^2-values are set to k_n^2. The new point (z^*_{n+m}, k_n^2) is also included. The procedure now restarts from the right on the ghost profile. After a number of detachments of wells, the ghost profile will eventually become a vertical line of points equal to the lower limit in (5.6), which means that all conceivable wells have been extracted. It should be noted that wells may be bounded by layer interfaces. If so, the ray is reversed by a reflection rather than a turning point. The ghost profile is never used for any ray computations. It is just a device of decomposing the wave number space such that $r(k_r)$ is smooth in each domain (5.4).

5.2.2 The eigenray problem in a sound channel

It remains to solve the range equation (5.1) in a k_r^2 domain (5.4), in which the rays will cycle up and down between two limits in depth. The minimum and maximum depth points of the ray are layer boundaries or turning points. The lower and upper bounds of all rays within the well are given by z_j and z_{j+1} in (5.4). In any case, the depths of the extrema of a ray can be found directly from the ghost profile. The smallest and largest depth range of all rays can be used to obtain an estimate of the smallest and largest range of any ray within the well. It can be done as follows. The steepest angle of a ray is determined by

$$(k_z)_{max} = \sqrt{k^2_{max} - k^2_{rj}},$$

which is applied layer by layer. By using the steepest possible angle, and the smallest cycling depth, an estimate of the shortest possible range can be estimated. If this range exceeds r_e, the well is void of eigenrays of the type under consideration. In the same way one can estimate the largest possible range using the largest cycling depth, k^2_{min} and $k^2_{r,j+1}$. These estimates, which are based on min and max speeds of layers, are useful when k_r is considerably smaller than k_{min}.

If the above estimates are inconclusive, $r(k_r)$ must be evaluated by ray tracing. It is done in an adaptive manner as follows. The k_r-interval is divided into a number of subintervals, which are stored in a stack and processed one by one in a uniform way. The stack grows and diminishes in a dynamic way, but ultimately it becomes empty when all eigenrays, if any, have been found. Let $dk_r = [k_r^L, k_r^R]$ be a subinterval to be searched. The first action is to evaluate the ranges at the endpoints, that is, $r(k_r^L)$ and $r(k_r^R)$. If the bracket condition (5.2) is fulfilled, the combined Newton/bisection method is applied to compute one root. Once done, a thin slice around the root is cut off from dk_r, and the remaining parts on each side of the cut are added to the stack. In the other case, that is, with $r(k_r^L)$ and $r(k_r^R)$ on the same side of r_e, a cubic Hermite interpolating polynomial $p(k_r)$ is formed using $r(k_r^L)$, $dr(k_r^L)/dk_r$ and $r(k_r^R)$, $dr(k_r^R)/dk_r$. The extrema

$$p_{min} = p(k_r^{min}) = min_{dk_r} p(k_r),$$
$$p_{max} = p(k_r^{max}) = max_{dk_r} p(k_r)$$

are determined analytically. Assume that

$$r(k_r^L) < r(k_r^R) < r_e.$$

Now if $p_{max} < r(k_r^R)$, then dk_r is declared void of eigenrays and removed from the stack. If $p_{max} > r(k_r^R)$, then dk_r is divided into two subintervals with k_r^{max} as a divider. They are added to the stack, while the parent interval is removed.

The stack is initialized by three subintervals

$$[r(k_{rj} + \epsilon), r(k_{rj} + \delta)], \quad [r(k_{rj} + \delta), r(k_{r,j+1} - \delta)], \quad [r(k_{r,j+1} - \delta), r(k_{r,j+1} - \epsilon],$$

where

$$\delta = 0.01(k_{r,j+1} - k_{rj})$$

and ϵ is a very small number to avoid possible singularities of the derivative of the range function at the endpoints. This is also the reason for the choice of using small subintervals around the endpoints.

5.2.3 An example of a caustic

A common feature of acoustic wave propagation in inhomogeneous media is focusing. In ray acoustics this phenomenon implies that nearby rays intersect and form a caustic surface in space. A typical example of a caustic is shown in Fig. 5.2.

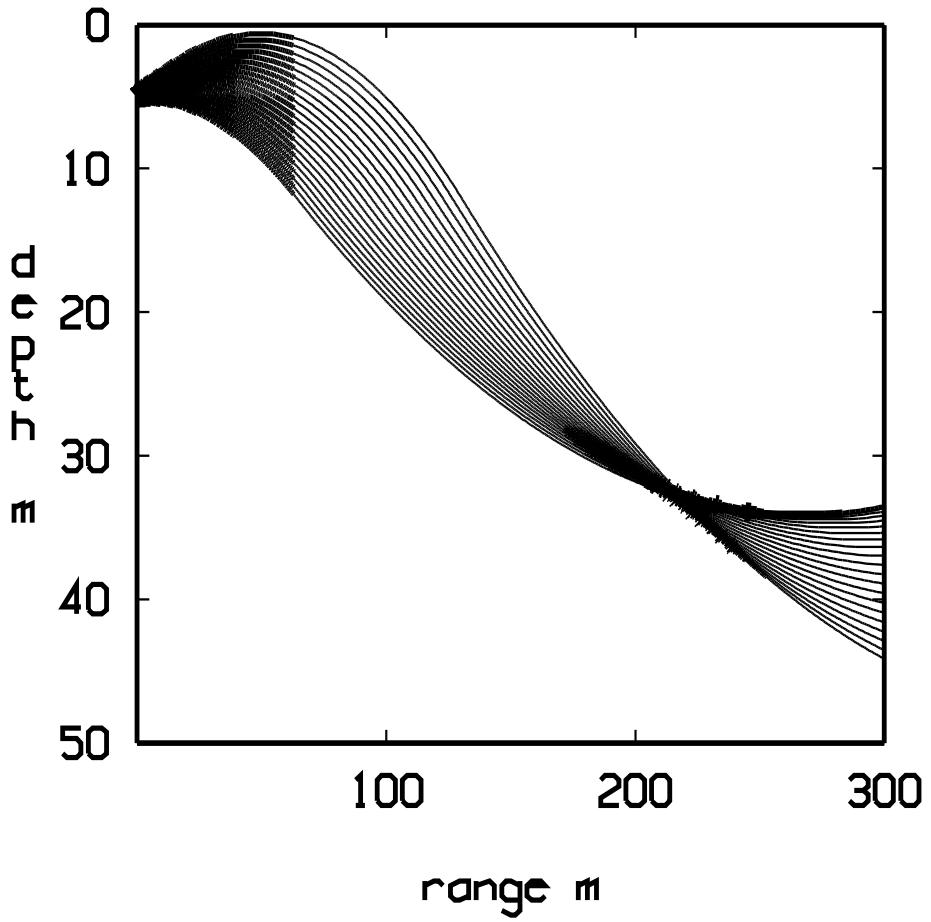

Figure 5.2: *This ray diagram shows the formation of a cuspoid caustic around* 200 m *from the source. The caustic is an envelope to a bundle of converging rays.*

A bundle of rays from a shallow source at $(0, 5)m$ are launched slightly upwards in a sea with the bilinear sound speed profile

$$(0, 1500), \quad (12, 1440), \quad (50, 1500), \quad [(m, m/s)].$$

At the point $(30, 200)$ m in the depth-range diagram the rays converge to a needle which splits into upper and lower boundaries. It is a caustic of the cuspoid family [9]. An expanded view of the caustic region is shown in Fig. 5.3.

The ray solution breaks down at the caustic, because infinite intensity is predicted. The caustic is the locus of points in which the range derivative dr/dk_r is zero. Figure 5.4 depicts the range function $r(k_r)$ versus a normalized k_r-interval corresponding to the search domain (5.4) for the depth $33m$ and the ray type -11 (surface-reflected or refracted rays).

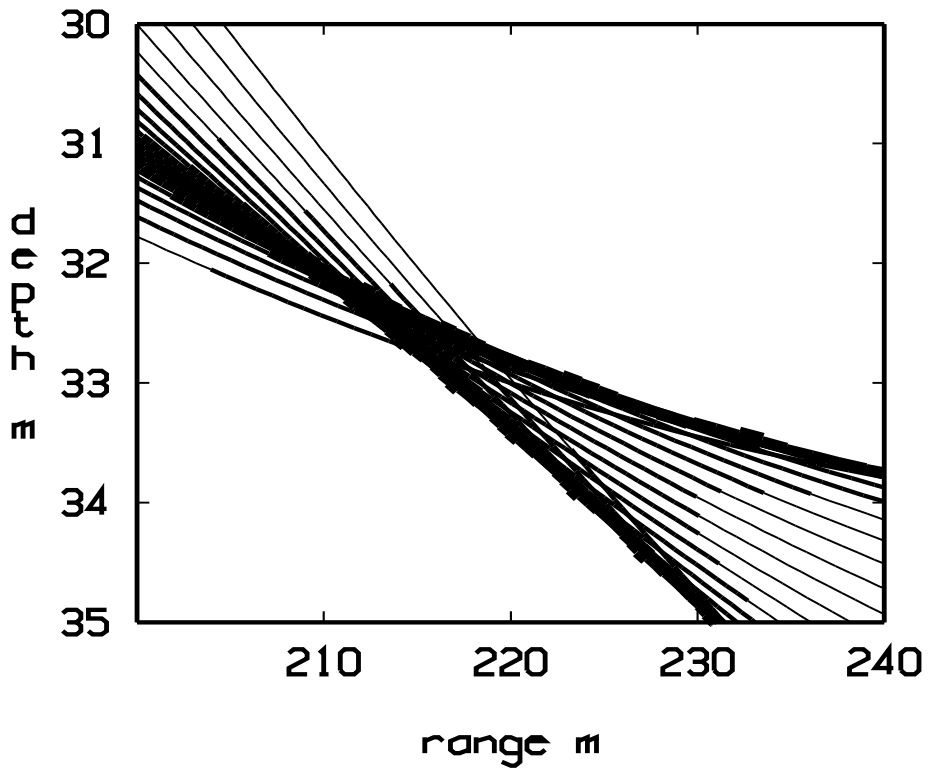

Figure 5.3: *The caustic has the form of a cusp, whose interior is covered by crossing rays giving rise to an interfering sound field of high intensity. The region outside the cusp is a shadow zone.*

There are two extrema of the range curve where the derivative is zero. The corresponding ranges $\approx 218m$ and $\approx 223m$ are points on the caustic for the depth $z = 33m$. The range interval between these points lies in the insonfied region.

When RAYLAB is called to compute the eigenrays of type -11 for a receiver at $(33, 220)m$, the result is given by Table 4.1.

No	Time,ms	TL	TLgeo	TLref	TLabs	Angle	ray id
1	152.11	32.9	32.9	0	0	-3.99	-11
2	152.09	36.5	36.5	0	0	-9.89	-11
3	152.09	61.8	61.8	0	0	-10.66	-11

Table 4.1. *Each ray is tabulated with arrival time, total transmission loss, losses due to geometrical spread, interfaces and absorption. The departure angle at the source and layers traversed by the ray are also listed.*

The first two eigenrays correspond to the intersection points with the horizontal line $r = 220m$ and the range curve in Fig. 5.4. The third eigenray is a surface reflected eigenray, which has nothing to do with the caustic. Its intensity is also quite small in comparison with the rays that touch the caustic.

This example illustrates some of the difficulties that may arise in finding eigenrays. Three eigenrays of the same type appear in a rather small k_r-interval.

The total number of calls to the subroutine that evaluates the range function is a

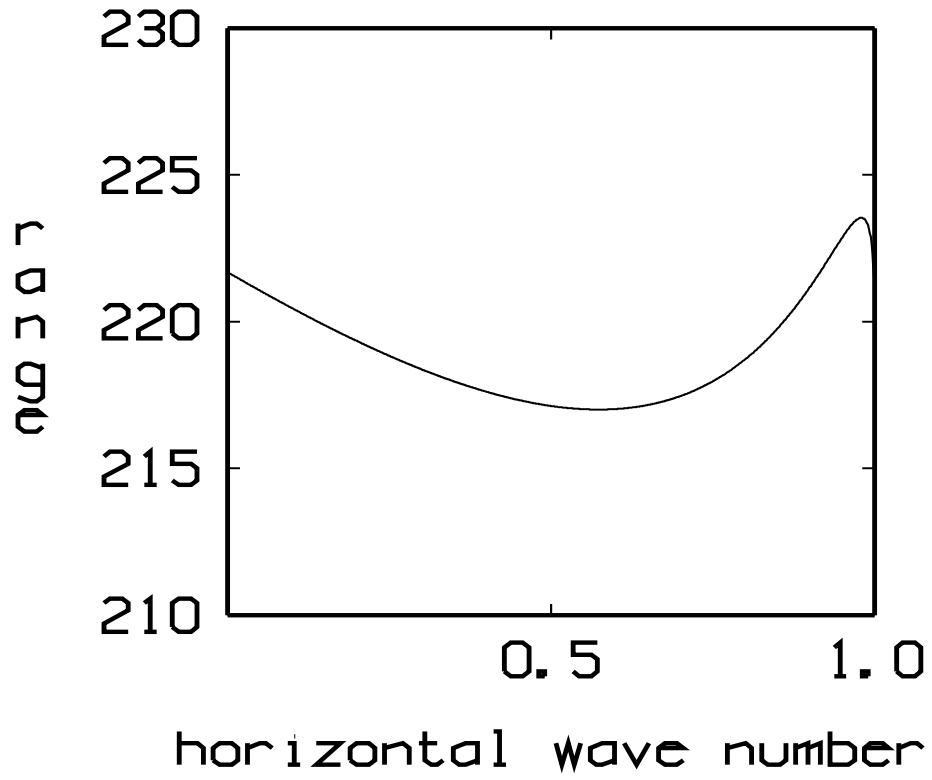

Figure 5.4: *The range function $r(k_r)$ for $z = 33m$ versus a normalized wave number spanning the search domain in solving the range equation (5.1). The two peaks at the ranges $\approx 218m$ and $\approx 223m$ lie on the caustic.*

measure of efficiency of the eigenray solver. In the present example 48 ray traces were done in order to find all three eigenrays.

6 Impedance calculations

In ray acoustics the sound field at a receiver is obtained by summing up complex pressure amplitudes of all waves associated with the eigenrays. The type and number of eigenrays needed must be decided prior to the run of RAYLAB. At short range only a few eigenrays are needed because ray angles rapidly become steeper as the number of reflections increases. Ultimately when the incident angle towards the half-infinite bottom is steeper than the critical angle of total reflection, a portion of energy is lost at each bottom bounce. At long range though, a comparatively larger number of rays travel at shallow angles and they suffer little from reflections at interfaces of high velocity layers. Then the computational cost, and the bookkeeping of all possible ray paths in a multilayered seabed, become an unbearable burden already at ranges beyond a few water depths. A sensible solution to this problem is to restrict the ray tracing to the water layer, and to use an effective reflection coefficient at the water/sediment surface. It is common to let this coefficient represent the combined wave response of the entire bottom stratification. It also means that the reflection coefficient becomes frequency dependent, since it embodies the characteristics of a multilayered bottom.

This approach is also made an option in RAYLAB.

The computations of the reflection coefficent due to a multilayered bottom is accomplished by using the impedance. This technique can be explained in terms of the depth-separated equation

$$\rho\frac{\partial}{\partial z}(\frac{1}{\rho}\frac{\partial\hat{u}}{\partial z}) + (k^2(z) - k_r^2)\hat{u}(z,k_r) = 0, \tag{6.1}$$

which is obtained by applying the Hankel transform to the Helmholtz equation (3.9) [5]. In this section we restore the frequency dependence of the wave number, that is, $k = \omega/c(z)$. The impedance at the depth z for a solution $\hat{u}$ of this equation is defined by

$$Z(z,k_r) = \frac{\hat{u}}{\frac{1}{\rho}\frac{\partial\hat{u}}{\partial z}}. \tag{6.2}$$

The impedance Z is continuous across layer boundaries, because it is the ratio of the complex pressure and normal particle velocity (apart from a factor $i\omega$). Let z_b denote the depth of the water. Then a downgoing wave incident on the bottom and the backreflected wave can be written as

$$\begin{aligned}\hat{u}(z,k_r) &= A\left(\exp^{ik_z(z-z_b)} + R\exp^{-ik_z(z-z_b)}\right)\\ \frac{\partial\hat{u}}{\partial z} &= ik_zA\left(\exp^{ik_z(z-z_b)} - R\exp^{-ik_z(z-z_b)}\right),\end{aligned} \tag{6.3}$$

where

$$k_z = \sqrt{k^2(z_b) - k_r^2}, \quad Im\sqrt{\ } \geq 0.$$

Here it is assumed that the media parameters ρ_w, c_w, α_w of the water are homogeneous in the vicinity of the bottom. Now by impedance matching at z_b, we obtain by using the relations (6.2) and (6.3)

$$\frac{1+R}{\frac{ik_z}{\rho_w}(1-R)} = Z(z_b,k_r)$$

or

$$R = -\frac{1-\frac{ik_z}{\rho_w}Z}{1+\frac{ik_z}{\rho_w}Z}. \tag{6.4}$$

It remains to compute the impedance of a stack of layers for an incoming wave from the top. It can be done by a down-up approach starting with a known impedance of the half-infinite bottom. The latter is obtained directly from the assumption of one-way propagation towards $+\infty$. In layers with constant parameters the solution can be written in the form (6.3), and the formula (6.4) can be applied to find a reflection coefficient one layer up. Once known, the impedance at the initial depth of the layer is found. In this way the impedance is propagated upwards layer by layer in a repetitive fashion. In layers with depth-dependent parameters, the expression (6.3) does not apply. Then as before, we introduce a piecewise linear approximation in each sublayer based on tabular data. The linearity of k^2 makes it possible to write the solution in terms of Airy functions [10]. A slight complication arises if the density is a piecewise

linear function of depth. This case is dealt with the transformation $\hat{u} = \sqrt{\rho}\tilde{u}$, for which the equation (6.1) goes over into

$$\frac{\partial^2 \tilde{u}}{\partial z^2} + (k^2(z) - k_r^2 + \frac{1}{2}\frac{\rho''}{\rho} - \frac{3}{4}\frac{(\rho')^2}{\rho^2})\tilde{u}(z, k_r) = 0. \tag{6.5}$$

The new wave number squared is now made a linear function in each sublayer by dropping ρ''. By an additional scaling of the depth coordinate z the equation (6.5) is transformed to the Airy equation. The Airy functions and their derivatives can be evaluated by a recently developed code [11].

A compact way of displaying the reflection coefficient is shown in Fig. 6.1. It is a color plot of the reflection loss in dB for the multilayered bottom described in Sec. 2.3.

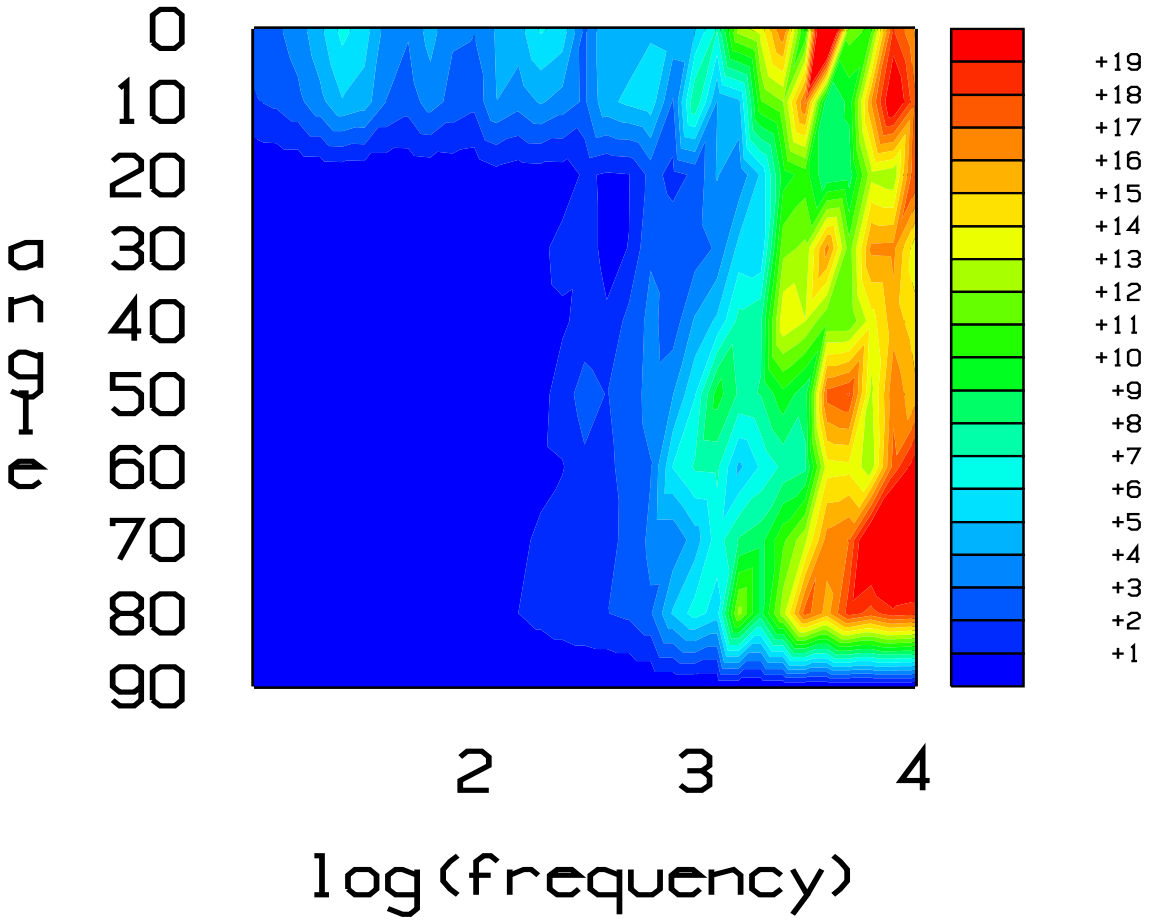

Figure 6.1: *The reflection loss* $-20log(R)$ *dB as function of frequency (Hz) and incident angle for the 3-layered bottom in Sec. 2.3.*

This map can be regarded as a geoacoustic signature of the bottom configuration. For example, a notable feature is that bottom loss increases strongly for frequencies above $\approx 1kHz$, except for waves with very small grazing angles.

6.1 A comparison with JEPE

We shall consider a computational example in which the ray tracing is restricted to the water, and the bottom is represented by an effective reflection coefficient. We also want to evaluate the ray solution against a reference solution generated by JEPE, which is a code based on the parabolic wave equation [12],[13]. In the present study it can be regarded as a comprehensive model of high fidelity. The geoacoustic profile is the same as before, that is, the one given in Sec. 2.3. A shallow source is placed at $(0, 5)m$ and a receiver at $(3000, 20)m$. The computational domain of JEPE was set to

$$0 \leq r \leq 3000, \quad 0 \leq z \leq 50$$

with a transparent boundary condition at $z = 50m$ [14]. The RAYLAB solution was based on 60 eigenrays, which was found to be enough for a converged ray solution.

Transmission loss was computed for 230 frequencies in the range $100Hz$ to $25kHz$. The RAYLAB (black) and JEPE (red) solutions are depicted in Fig. 6.2. The computational time of the RAYLAB solution was $5s$, while the JEPE solution was an overnight run.

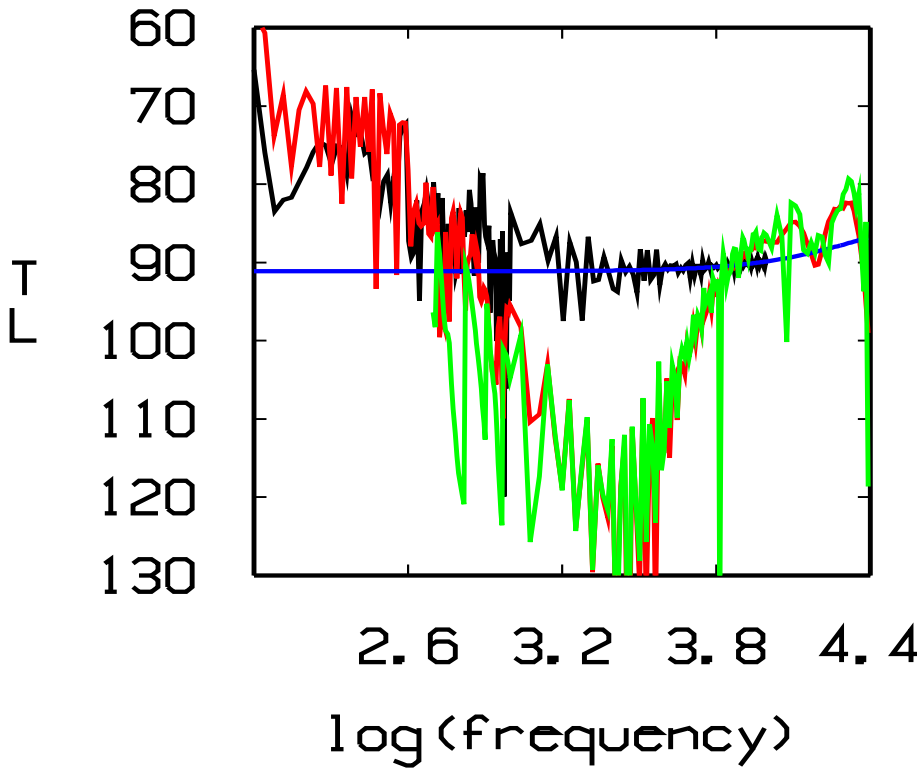

Figure 6.2: *Transmission loss as function of frequency (Hz) computed by RAYLAB (black) and JEPE (red). The blue curve is a RAYLAB solution with only the direct and surface reflected rays. The green curve is a MODELOSS solution based on modes with phase velocities in the range* $(1480, 1500)m/s$.

There is a striking disparity in transmission loss (TL) in the range $1 - 4kHz$, while the ray solution is mostly acceptable outside this range. An explanation is offered

by the blue and green TL curves. They show that the solution above $\approx 1kHz$ is determined by a few degrees of freedom. TL of the direct and surface reflected rays amount to $97dB$ respectively $87dB$ for high frequencies (tables of TL are not shown here). The influence of all other rays diminish by increasing frequencies. The reason is that they hit the bottom at grazing angles larger then 15°, because of the downward refracting profile and the shallow source. It means that they suffer a considerable reflection loss according to Fig. 6.1. In order to understand the intensity drop of the JEPE solution, it is helpful to look at the modal properties of the wave field. From a table of horizontal wave numbers of the modes (not shown here) it is found that only a few modes contribute to the field for frequencies larger than $\approx 1kHz$. This is also confirmed by computing a mode solution composed of modes with phase velocities in the narrow range $(1480, 1500)m/s$ (green curve). Their propagation angles, and depth penetration into the top sediment, decrease gradually as the frequency increases. At sufficiently large frequencies they suffer little from the absorption of the sediment and the intensity becomes higher. Decreasing mode angles and sediment penetration at higher frequencies is one manifestation of diffraction, and it has no counterpart in the ray model. For frequencies in which the wave propagation is not dominated by diffraction effects, there is a good agreement between the RAYLAB and JEPE solutions.

7 Time series simulations

Basically RAYLAB is a frequency domain code, and receiver time series are synthesized by an inverse Fourier transform of the product of the transfer function and the source spectrum. The transfer function is obtained by adding complex pressure values for the amplitude and phase of all eigenray solutions. It must be done for all frequencies of the spectrum of the emitted pulse. However, the most expensive task, namely, the computation of the eigenrays does not depend on the frequency, and the same ray paths can be used for all frequencies.

In RAYLAB it is left to the user to specify what types of eigenrays to be included, as well as to determine a time-window at the receiver. Both questions can be explored by some trial and error calculations in the frequency domain prior to the time simulations. The tables of travel times and losses make it easy to decide on a suitable set of eigenrays and time-window. The possibilty to generate a time-series for any set of rays is a unique feature of the ray model, which is helpful for the interpretation of measured data.

7.1 A comparison with MODELOSS

The following example has a double purpose. One objective is to compare the simulated time-series of RAYLAB and MODELOSS [15], [16]. The latter program, which is based on the method of normal modes, is a consolidated code being used for a long time. Second, a sample run that illustrates the essential characteristics of inversion in the time domain, is worthwhile.

The environmental description in Sec. 2.3 is used. The source and receiver are deployed $5m$ from the seabottom, that is, at the depth $17.5m$. The separation distance is $25m$.

The transmit pulse is a Ricker pulse with the center frequency $2kHz$ having a duration of $\approx 1ms$. The eigenrays selected were those depicted in Fig. 7.1.

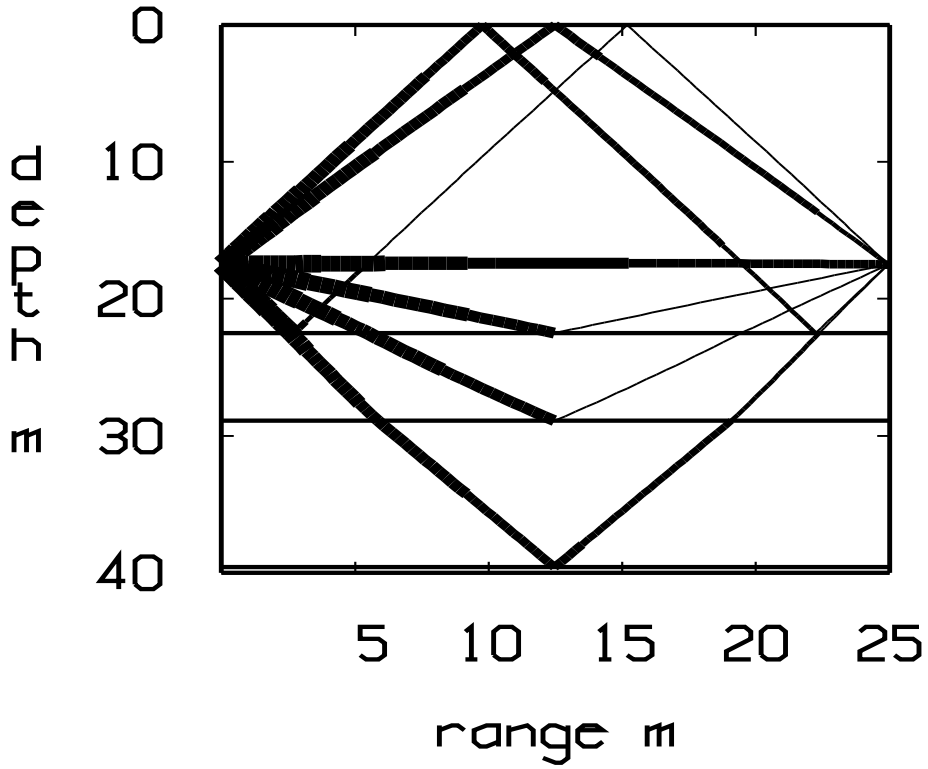

Figure 7.1: *This ray diagram shows the most important rays when the source and receiver are located* $5m$ *above the seabottom.*

The corresponding arrival times and loss factors are listed in Table 6.1.

No	Time,ms	TL	TLgeo	TLref	TLabs	Angle	ray id
1	17.20	28.0	28.0	0	0	-1.06	-11
2	18.59	49.1	28.4	20.7	0	21.31	11
3	23.42	48.2	30.5	13.8	3.9	42.04	1221
4	29.02	32.9	32.9	0	0	-55.24	-11
5	32.88	41.4	34.9	0.5	6.0	62.60	123321
6	34.90	49.5	34.4	15.1	0	61.39	111
7	34.92	49.5	34.4	15.1	0	-61.41	-111

Table 6.1. *Each ray is tabulated with arrival time, total transmission loss, losses due to geometrical spread, interfaces and absorption. The departure angle at the source and layers traversed by the ray are also listed.*

Figure 7.2 shows the computed time-series at the receiver by RAYLAB (black) and MODELOSS (red). The RAYLAB solution was obtained at immediate response, while the processing time of MODELOSS amounted to three minutes. The predictions are similar, except for the first arrival. The reason can be explained by the way the sound speed profile is interpreted by the codes. The direct ray is curved due to a slightly downward refracting profile at the depth of the source and receiver. A closer

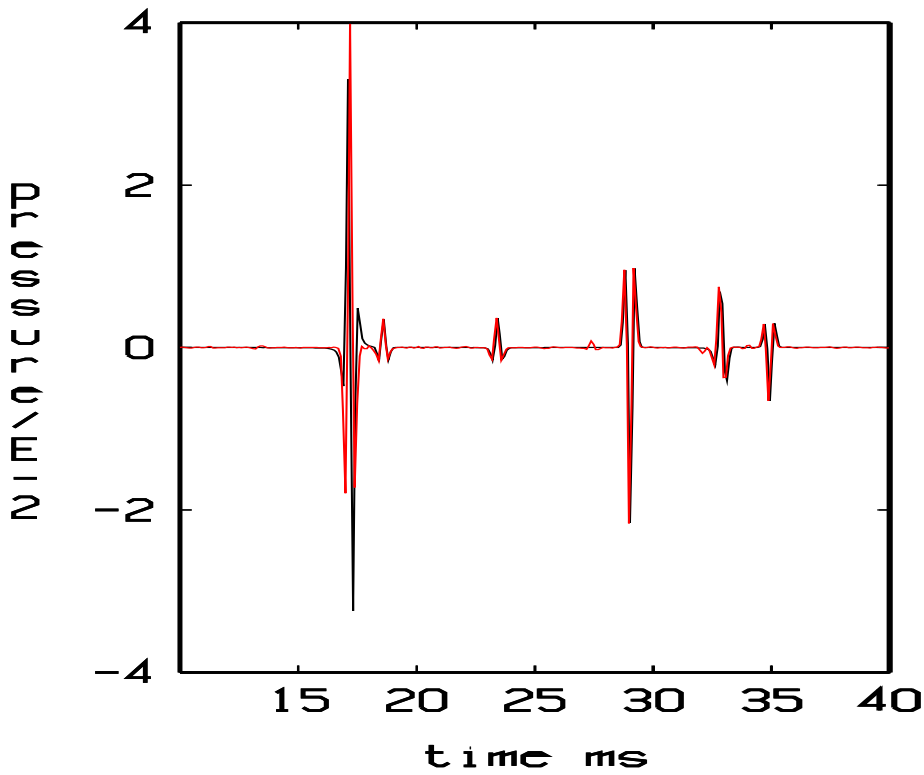

Figure 7.2: *The simulated time-series of RAYLAB (black) and MODELOSS (red).*

look at the ray path (not shown here), reveals that this ray touches a caustic. As a consequence the received pulse is a Hilbert tranform of the emitted one. MODELOSS is less sensitive to fine variations of the sound speed profile for two reasons. The profile is approximated by a staircase function, and diffraction effects due to finite frequency are retained in MODELOSS. The first arrival of the MODELOSS solution resembles a replica of the transmit pulse. Like the previous example in Sec.5.1, diffraction is of concern for horizontal propagation, and it affects the fidelity of the ray model. It should be noted though, that the prediction of arrival time is correct. Fortunately, the inversion will be based on steep rays for which the agreement is excellent, as can be seen from Fig. 7.2.

Next imagine that Fig. 7.2 is a measured signal at a site with unknown bottom properties. The task is to predict sub-bottom parameters. The first thing to be noted is that the peaks at the arrival times of the rays -11, 11, -11, 111, -111 in Table 6.1 are easy to identify. These rays have only traversed the water layer in which all propagation conditions are known. The direct ray at $17ms$, and the surface reflected ray at $29ms$, are the stongest ones. The wave form of the latter is flipped due to the reflection at the air/sea surface. Although these two arrivals do not contribute information about the bottom, they set a time-frame for the inversion. In addition, they can be utilized to determine the position of the receiver both in range and depth. The hitherto unidentified arrivals at $23ms$ and $33ms$ must be interpreted as reflections from sub-bottom interfaces. If similar reflections are observed at another receiver with a different separation distance, we obtain two pairs of arrival times. This information suffices to determine layer thicknesses and average speeds of two layers [1]. Once the

speed of the top layer has been determined, its density could be estimated by the amplitude of the bottom reflected arrival 11 at $18ms$. The reflection loss $20.7dB$ in Table 6.1 is available by subtracting the known geometrical loss from the total loss. The density is now obtained by using the expression for the reflection coefficient. The next targets are the absorption of the top sediment and the density of the bottom sediment. They could be determined from 1221 arrivals at two receivers. The crucial ingredient of this approach is the sorting of arrivals, and the decomposition of the total loss into its constituents. It remains to find out how the wave forms could be exploited for inversion. Inversion based on wave form analysis, rather than arrival times and amplitudes, has recently been performed in marine electromagnetics [17].

8 Forthcoming work

The flashing speed of a ray code makes it a key tool in exploring sonar data in real time. It should be remembered though, that certain loss of model fidelity has been traded for speed. Diffraction effects tend to be more pronounced for horizontal propagation. One specific shortcoming of importance for inversion is the absence of lateral waves in the ray model. Lateral waves travel horizontally in the vicinity of layer interfaces. They decay quickly by range, and they are excited only by radiation at critical angles. However, once captured they carry rich information on media contrasts across the interface. Incorporating lateral wave capabilities could be done with modest efforts as opposed to a comprehensive treatment of diffraction.

Developing a computational module for a systematic search of all caustics is an interest in its own. Maps of locations, types and stability properties with respect to media parameters would enrich our understanding of sound fields. Probably it could also be put to good use for inversion. There is much evidence that there is a strong velocity gradient in the upper $10m$ of the seafloor . This is a prerequisite for a caustic, which likely would appear in the water volume. Such a feature, if detected, would provide information on the velocity profile of the bottom sediment.

Shear wave profiles may be introduced into the impedance calculations. It would result in an effective reflective coefficient which embodies effects of partial conversion of compressional waves to shear waves at sediment interfaces. One could also compute eigenrays with shear wave segments in the sediments, although this would require a considerably larger effort.

A major problem is how to model small scale heterogeneities of the sediments, whose effects become more pronounced at higher frequencies. Amending the geoacoustic profile with scattering features must be combined with experimental studies in order to find an appropiate statistical description of sub-bottom scattering.

The rapid processing time of simulating time-series makes it possible to visualize wave phenomena like refraction, focusing, wavefront progression etc. by moving pictures. Such options could be added to simulation tools like COMBIS [18].

A sonar system for sediment classification under transit must be fully automated concerning two-fish, transmitter and receiver positions, adaptive control of separation distances and pulse shapes with respect to varying bathymetry and sediment thicknesses,

data acquisition and processing, inversion techniques and timing of operations. Each block in turn may be broken into a number of subtasks. For example, RAYLAB would be just one box of the flowchart of the software package for inversion. From a systems perspective, most work lies ahead.

References

[1] L. Abrahamsson, B.L. Andersson, I. Karasalo, and P. Sigray. Environment assessment for underwater sensors in the Stockholm archipelago, part 1 - inversion of hydroacoustic sub-bottom parameters. User report FOI-R–0706–SE, 2002.

[2] J.B. Keller. The geometrical theory of diffraction. *J. Opt. Soc. Amer.*, 52:116–130, 1962.

[3] S.J. Chapman, J.M.H. Lawry, J.R. Ockendon, and R.H. Tew. On the Theory of Complex Rays. *SIAM Rev.*, 41:417–509, 1999.

[4] V. Červený, M.M. Popov, and I. Pšenčík. Computation of wave fields in inhomogeneous media - Gaussian beam approach. *Geophys. J.R. astr. Soc.*, 70:109–128, 1982.

[5] F.B. Jensen, W.A. Kuperman, M.B. Porter, and H. Schmidt. *Computational Ocean Acoustics*. AIP Press, New York, 1994.

[6] G.B. Whitham. *LINEAR AND NONLINEAR WAVES*. J. Wiley, 1974.

[7] D.A. Sachs and A. Silbiger. Focusing and Refraction of Harmonic Sound and Transient Pulses in Stratified Media. *J. Acoust. Soc. Amer.*, 49:824–840, 1971.

[8] E.K. Westwood and P.J. Vidmar. Eigenray finding and time series simulation in a layered- bottom ocean. *J. Acoust. Soc. Amer.*, 81:912–924, 1987.

[9] M.G. Brown. The transient field in the vicinity of the cuspoid caustics. *J. Acoust. Soc. Amer.*, 79:1367–1384, 1986.

[10] L. Brekhovskikh and Yu. Lysanov. *Fundamentals of Ocean Acoustics*. Springer-Verlag, 1982.

[11] A. Gil, J. Segura, and N.M. Temme. Algorithm 819: AIZ, BIZ: Two Fortran 77 Routines for the Computation of Complex Airy Functions. *ACM Trans. Math. Softw.*, 28:325–336, 2002.

[12] L. Abrahamsson, L. Andersson, I. Karasalo, and A. Sundström. JEPE - a PE code for range-dependent fluid media. In *18th Scandinavium Symp. in Physical Acoustics*, pages 1–3. University of Bergen, Norway, 1995.

[13] I. Karasalo and A. Sundström. JEPE - a high-order PE-model for range-dependent fluid media. In *Proc. 3rd European Conference on Underwater Acoustics*, pages 189–194, Heraklion, Crete, Greece, 1996.

[14] P. Karlsson. Transparent boundary conditions for parabolic wave equations. Methodology report FOA-R-00-01752-409–SE, 2001.

[15] J. Pihl and L. Abrahamsson. MODELOSS - A User Oriented Code for Transmission Loss Calculations. FOA report R-95-00173-2.2-SE, 1995.

[16] L. Abrahamsson. Impedance boundary conditions for horizontally stratified media. Scientific report FOA-R-00-01424-409-SE, 2000.

[17] L. Abrahamsson, D. Berg, L. Crona, and P. Sigray. Determination of seabed conductivity by transient VLF sounding. in preparation, 2003.

[18] R. Sigg and J. Schiöld. COMBIS - version 2.0. Technical report FOI-R–0947–SE, 2003.